arXiv:1203.4286v1 [nucl-th] 19 Mar 2012

Constraining the Symmetry Parameters of the Nuclear Interaction

J. M. Lattimer[1,*] and Y. Lim[1,†]

[1]*Department of Physics and Astronomy, Stony Brook University, Stony Brook, NY 11794-3800, USA*

We show combining nuclear mass data with experimental information from neutron skins, heavy ion collisions, giant dipole resonances and dipole polarizabilities, and theoretical calculations of neutron matter, lead to stringent constraints on the symmetry properties of the nuclear interaction near the nuclear saturation density. Furthermore, these constraints are remarkably consistent with inferences from astrophysical observations of neutron stars. The concordance of experimental, theoretical and observational analyses suggests that neutron star radii, in the mass range 1 $M_\odot$ – 2 $M_\odot$, lie in the narrow window 11 km $< R <$ 12 km.

PACS numbers: 26.60.Kp, 97.60.Jd, 21.65.Cd

Introduction.– The nuclear symmetry energy, and in particular its density dependence, has been the focus of much recent activity due to its importance to astrophysics [1]. The expected neutino signal from gravitational collapse supernovae within our Galaxy is sensitive to the symmetry energy both before core bounce [2] and at later times from proto-neutron stars [3]. The radii of neutron stars are closely correlated to the pressure of neutron star matter in the range $n_s - 3n_s$ [4], and therefore to the density derivative of the symmetry energy at the nuclear saturation density n_s. Neutron star radii strongly affect both moments of inertia [5] and the expected gravitational signals from mergers involving neutron stars [6]. The composition of matter at densities above n_s, and the existence of neutrino processes which can rapidly cool neutron stars, depends on the density dependence of the symmetry energy [7], as do the properties of neutron-rich nuclei and reaction rates involved in the astrophysical r-process. The symmetry energy controls properties of neutron star matter below n_s, such as the core-crust transition density in neutron stars which is important in pulsar glitches [8], crust relaxation in cooling [9] and accreting [10] neutron stars, and astroseismology from giant magnetar flares [11].

Nuclear Symmetry Energy.– The nuclear symmetry energy is alternatively expressed in one of two ways: as the difference S between the energies of pure neutron and isospin symmetric matter, $S(u) = e(u, 0) - e(u, 1/2)$, where $e(u, x)$ is the energy per baryon of nuclear matter with baryon density $n = un_s$ and proton fraction x, or as the coefficient S_2 of a quadratic expansion of symmetric matter in the neutron excess,

$$e(u, x) = e(u, 1/2) + S_2(u)(1 - 2x)^2 + \dots . \qquad (1)$$

It is often assumed that $S \simeq S_2$ but this need not be true. While the kinetic contributions from non-interacting nucleons lead to a small difference,

$$\delta S_{kin}(u) \equiv S_{kin}(u) - S_{2.kin}(u) \simeq 0.72u^{2/3} \text{ MeV}, \qquad (2)$$

there is no guarantee that potential energy contributions are similarly small. Many Skyrme interactions were constructed with the property that their potential energy contributions to δS_{pot} vanish, but some other Skyrme interactions have unphysical neutron matter properties at high densities due to large potential energy contributions.

It is customary to define the liquid droplet symmetry energy parameters S_v, L and K_{sym}:

$$\begin{aligned}
S_v &= \frac{1}{8}\left(\frac{\partial^2 e}{\partial^2 x}\right)_{u=1,x=1/2} = S_2(1), \\
L &= \frac{3}{8}\left(\frac{\partial^3 e}{\partial u \partial^2 x}\right)_{u=1,x=1/2} = \frac{3}{8}\left(\frac{dS_2}{du}\right)_{u=1}, \qquad (3) \\
K_{sym} &= \frac{9}{8}\left(\frac{\partial^4 e}{\partial u^2 \partial^2 x}\right)_{u=1,x=1/2} = \frac{9}{8}\left(\frac{d^2 S_2}{du^2}\right)_{u=1}
\end{aligned}$$

While these parameters are not useful in describing the nuclear symmetry energy far from the saturation density, most astrophysical applications are most sensitive to the symmetry energy near the saturation density. There are limited constraints on K_{sym} from measurements of the giant isoscalar monopole resonance [12], isotopic transport ratios in medium-energy heavy ion collisons [13], and neutron skin data from anti-protonic atoms [14], but extraction of the symmetry contribution to the total incompressibility of nuclei and its separation into bulk (K_{sym}) and surface contributions is still problematic.

In contrast, there are several experiments leading to effective constraints on S_v and L, including nuclear mass fitting, neutron skins, dipole polarizabilities, dynamics in heavy ion collisions, giant and pygmy dipole resonances, and isobaric analog states.

Nuclear Mass Fitting.– The most accurate and least ambiguous data are nuclear masses. However, optimizing the values of symmetry parameters from experimentally-measured masses cannot uniquely constrain them due to their significant correlation [15]. This can be easily observed by referring to the standard liquid drop model [16] in which the symmetry energy of an isolated nucleus is $E_{drop,A} = I^2(S_v A - S_s A^{2/3})$ where $I = (N - Z)/(N + A)$ is the neutron excess. The bulk symmetry parameter S_v is identical to that appearing in Eq. (3). S_s is the surface symmetry energy parameter which depends on the behavior of S within the surface and thus S_v, L and K_{sym}. The correlation follows from minimizing the difference between the model and experimentally measured symmetry energies, i.e., minimizing $\chi^2 = \sum_i (E_{exp,i} - E_{drop,i})^2/(\mathcal{N}\sigma^2)$, where $\mathcal{N}$ is the total number of nuclei and σ a nominal error. A contour of χ^2 one unit above the minimum value represents a 1σ confidence ellipse. The properties of the ellipse are determined by the second derivatives of χ^2 at the minimum,

$$\begin{aligned}[\chi_{vv},\ \chi_{vs},\ \chi_{ss}]\sigma^2 &= \frac{2}{\mathcal{N}}\sum_i I_i^4[A_i^2,\ -A_i^{5/3},\ A_i^{4/3}] \\ &\simeq [61.6,\ -10.7,\ 1.87], \end{aligned} \qquad (4)$$

where $\chi_{vs} = \partial^2\chi^2/\partial S_v \partial S_s$, etc. In this simple example, these derivatives depend only on A_i and I_i, not the location of the χ^2 minimum. The confidence ellipse in $S_s - S_v$ space has orientation $\alpha = (1/2)\tan^{-1}|2\chi_{vs}/(\chi_{vv} - \chi_{ss})| \simeq 9.8°$ with respect to the S_s axis, with error widths $\sigma_v = \sqrt{(\chi^{-1})_{vv}} \simeq 2.3\sigma$ and $\sigma_s = \sqrt{(\chi^{-1})_{ss}} \simeq 13.2\sigma$ where (χ^{-1}) is the matrix inverse, and a correlation coefficient $r = \chi_{vs}/\sqrt{\chi_{vv}\chi_{ss}} \simeq 0.997$.

It is necessary to transform the correlation between S_s and S_v into one between L and S_v. Treating the nuclear surface as a plane-parallel interface, to lowest order S_s can be expressed as the ratio of two integrals over the density profile $u = n/n_s$ of a symmetric system [1]:

$$\frac{S_s}{S_v} = \frac{E_s}{2}\frac{\int_0^1 u^{1/2}[S_v/S_2(u) - 1]f(u)^{-1/2}du}{\int_0^1 u^{1/2}f(u)^{1/2}du}, \qquad (5)$$

where $f(u) = e(u, 1/2) + B,\ B = -e(1, 1/2) \simeq 16$ MeV is the bulk symmetric binding energy at n_s, and $E_s \simeq 19$ MeV is the liquid drop surface energy parameter (also estimated from fitting nuclear masses). The transformation depends on S_2 and e and is generally complex, but an analytical result is found if we approximate $S_2(u) \simeq S_v + L(u-1)/3$ and $f(u) \simeq K_o(u-1)^2/18$, where $K_o \simeq 240$ MeV is the incompressibility:

$$S_s/S_v \simeq 135 E_s \left[1 - \beta\tan^{-1}\beta^{-1}\right]/(2K), \qquad (6)$$

where $\beta = \sqrt{3S_v/L - 1}$. With $L/S_v = 1,\ 3/2,\ 2$, one finds $S_s/S_v \simeq 0.7,\ 1.2,\ 1.8$ which shows the basic trend. A much better approximation comes from semi-infinite Thomas-Fermi calculations [17]:

$$\frac{S_s}{S_v} \simeq 0.0555 + \frac{S_v}{88.1\mathrm{MeV}} + 1.42\frac{L}{S_v} + 0.423\left(\frac{L}{S_v}\right)^2. \qquad (7)$$

Transforming to $S_v - L$ space, one finds a confidence ellipse with $\sigma_v \simeq 2.3\sigma$ and $\sigma_L \simeq 23\sigma$.

In practice, the liquid droplet model [19], which accounts for varying neutron/proton ratios within the nucleus, represents an improved treatment of the total nuclear energy. Its symmetry energy is $E_{LD,A} = I^2 S_v A(1 + S_s A^{-1/3}/S_v)^{-1}$ and therefore predicts a linear correlation between S_s/S_v and S_v. The same methodology as for the drop model can be used to determine the confidence ellipse. One ultimately finds $\sigma_v \simeq 2.7$ MeV and $\sigma_L \simeq 37$ MeV if $\sigma = 0.5$ MeV (these values now depend on the location of the minimum, $S_{v0} \simeq 29.6$ MeV and $L_0 \simeq 47$ MeV, with shell and pairing effects taken into account). As shown in Fig. 1, the centroid and orientation are in remarkable agreement with a recent Hartree-Fock fit to experimental masses and radii using a parametrized energy-density functional (EDF) [20], which finds $S_{v0} \simeq 30.5$ MeV and $L_0 \simeq 45$ MeV. The RMS error of the EDF fit is approximately 1.45 MeV, with $\sigma_v = 3.1$ MeV and $\sigma_L = 40$ MeV; these values are similar to those of the liquid droplet fit if $\sigma \approx 0.5$ MeV. A parametrized finite-range Thomas-Fermi (FRTF) model for nuclei produces a nearly identical result [17]. The correlation of S_v and L is approximately 97% in the EDF fit, smaller than the correlation of the liquid droplet fit since the EDF model was also constrained by nuclear radii.

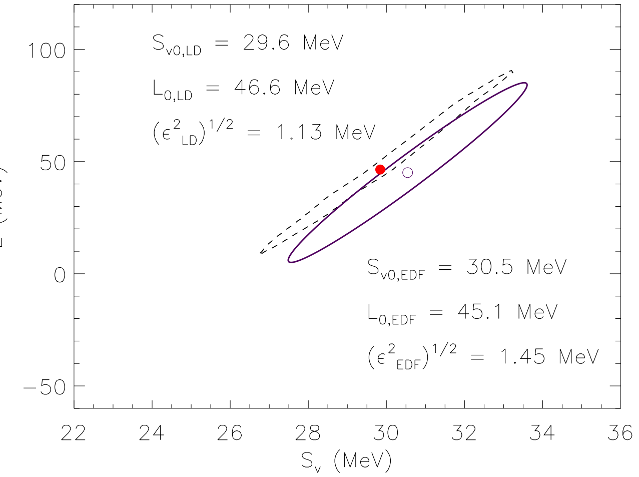

FIG. 1: Comparison of confidence ellipses for nuclear mass fitting. The solid ellipse is the EDF 1σ result of Kortelainen et al. [20] and the dashed ellipse is the liquid droplet model result assuming $\sigma = 0.5$ MeV. The quantities S_{v0} and L_0 (plotted as circles) are the minimum χ^2 values and $(\epsilon^2)^{1/2}$ are the RMS errors of the respective fits.

The high degree of correlation of the symmetry parameters established from nuclear mass fitting has already been used to constrain equation of state tables [18], but can be combined with data from other experiments to produce even greater constraints.

Other Experimental Constraints.– The liquid droplet model implies that other nuclear observables will be related to the surface and volume symmetry coefficients. An example is the neutron skin thickness of neutron-rich nuclei. Neglecting Coulomb effects, the difference between the mean neutron and proton surfaces in the liquid droplet model [19] is

$$t_{np} = \frac{2r_o}{3}\frac{S_s I}{S_v + S_s A^{-1/3}}, \qquad (8)$$

which is primarily a function of S_s/S_v. It should then form a nearly orthogonal constraint to that from nuclear masses. Values of t_{np} have been measured, typically with 30-50% errors, for a few dozen nuclei. A recent study of Sn isotopes [21], where differential measurements with fixed Z can reduce errors, found the correlation between S_v and L plotted in Fig. 2. It is nearly orthogonal to the mass-fit correlation (the 95% confidence ellipse from Ref. [20] is shown in Fig. 2). First results [22] from the PREX experiment to measure the neutron skin of ^{208}Pb are too imprecise to be definitive as they imply $35 < L/\mathrm{MeV} < 262$ for reasonable values of S_v. The central value of L is discrepant with other results for neutron skins, but the uncertainties are still very large.

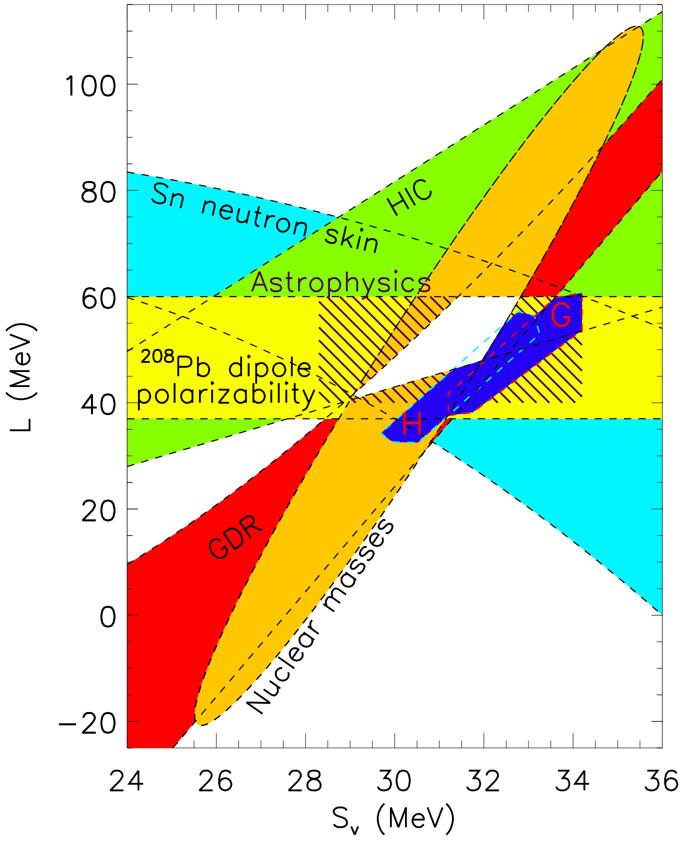

FIG. 2: Summary of constraints on symmetry energy parameters. The filled ellipsoid indicate joint $S_v - L$ constraints from nuclear masses [20]. Filled bands show constraints from neutron skin thicknesses of Sn isotopes [21], the dipole polarizability of Pb [25], giant dipole resonances [17, 26], and isotope diffusion in heavy ion collisions [27]. The hatched rectangle shows constraints from fitting astrophysical $M - R$ observations [37]. The two closed regions show neutron matter constraints (H is Ref. [33] and G is Ref. [34]). The white area is the experimentally-allowed overlap region.

The hydrodynamical model of Ref. [23] showed that both the dipole polarizability and the giant dipole resonance centroid energy are closely connected to liquid droplet parameters. The centroid energy is

$$E_{-1} \simeq \sqrt{\frac{3\hbar^2(1+\kappa)}{m<r^2>} S_v \left(1+\frac{5}{3}\frac{S_s}{S_v}A^{-1/3}\right)^{-1}}, \qquad (9)$$

where κ is an enhancement factor arising from the velocity dependence of the interaction and $< r^2 >$ is the mean-square charge radius. The factor $m < r^2 > /(1+\kappa)$ does not significantly vary among interactions for a given nucleus. As a result, a series of measurements of the GDR among various nuclei should result in a correlation between S_s/S_v and S_v that is similar to but slightly less steep than that from nuclear masses. The liquid droplet model predicts the orientations of the correlations in the $S_s/S_v - S_v$ plane will have the ratio

$$\frac{\alpha_{GDR}}{\alpha_{masses}} \approx \frac{5}{3}\left(1+\frac{5}{3}\frac{S_{s0}}{S_{v0}} < A^{-1/3} >\right)^{-1} \simeq 1.4, \qquad (10)$$

where $<>$ refers to an average over the measured nuclei. Using a variety of Skyrme functions, Trippa, Cólo & Vigezzi [26] show the GDR in ^{208}Pb implies that $S_2(u)$ evaluated at the density $n = 0.1$ fm^{-3} is limited to $23.3 < S_{2,0.1}/\mathrm{MeV} < 24.9$. While the connection between $S_{2,0.1}$ and S_v and L is model dependent, bounds for a range of parametrizations [17] are indicated in Fig. 2. The correlation band has a shallower slope, compared to that from masses, as expected from the droplet model.

Tamii et al. [24] established the limit $23 < L/\mathrm{MeV} < 54$ from measurements of the dipole polarizability of ^{208}Pb. A systematic analysis incorporating model dependencies [25] revised this range to $37 < L/\mathrm{MeV} < 60$, and is shown in Fig. 2.

Constraints from heavy ion collisions include those from isospin diffusion [27], shown in Fig. 2, and from multifragmentation in intermediate-energy heavy ion collisions [32]. The latter implies $40 < L/\mathrm{MeV} < 125$ but is not displayed in Fig. 2 for clarity.

Not included in Fig. 2 are results of a study of pygmy dipole resonances [28] in ^{68}Ni and ^{132}Sn which imply $31 < S_v/\mathrm{MeV} < 33.6$ and $49.1 < L/\mathrm{MeV} < 80$. Daoutidis & Goriely [29] argue that theoretical and experimental uncertainties prevent them from being effective constraints. The results of Reinhard & Nazarewicz [30] confirm pygmy resonance energies lack significant correlation with L.

Danielewicz & Lee [31] proposed isobaric analog states as constraints on symmetry parameters, leading to $S_v \simeq 33$ MeV and $S_s \simeq 96$ MeV, which is equivalent to $L \simeq 113$ MeV. However, the data suggest there is a significant curvature contribution; re-fitting with curvature yields $S_v \sim 30$ MeV and $S_s \sim 45$ MeV, equivalent to $L \sim 50$ MeV, but with considerable errors [17]. A more detailed analysis is necessary to produce better constraints.

In summary, the various experimental results are consistent with each other, and they jointly confine the allowable ranges of symmetry parameters to the small white overlap region in Fig. 2.

Neutron Matter and Astrophysical Studies.– Recent studies of pure neutron matter have employed chiral lagrangian [33] and quantum Monte Carlo [34] techniques using realistic two- and three-nucleon interactions. The energies and pressures of neutron matter at n_s, if quartic and higher order symmetry energy contributions can be neglected, are $e(1,0) = S_v - B$ and $p(1,0) = Ln_s/3$. Despite the different theoretical approaches, and considering physically-motivated ranges for interaction strengths, the neutron matter predictions for the symmetry parameters are consistent with each other and with experimental studies, as shown in Fig. 2.

Neutron star radii are highly correlated with neutron matter pressures near n_s [4]. Quiescent neutron stars in globular clusters [35] provide information concerning their apparent angular radius, R_∞/D, where $R_\infty = R(1-2GM/Rc^2)^{-1/2}$ and M and R are the stellar mass and radius. Although the distances D are only approximately known, these sources are believed to have well-understood H-dominated, low magnetic field, atmospheres. Type I X-ray bursts on neutron star surfaces [36] provide, in addition to angular sizes, measured maximum fluxes thought to be near the Eddington limit $F_{Edd} = cGM/(\kappa D^2)$ (neglecting redshift) at which radiation pressure balances gravity (κ is the opacity). For these sources, major uncertainties include distances as well as atmospheric properties. Despite estimated errors in M and R of order 20% or more for each source, a Bayesian analysis [37] of an ensemble of both types of sources implies $11 < R/\mathrm{km} < 12$ for masses between 1.2 and 2 $\mathrm{M}_\odot$, and $40 < L/\mathrm{MeV} < 60$ (see Fig. 2). Interestingly, pulse-shape modeling [38] of accreting millisecond pulsars produces a virtually identical constraint.

Conclusions.– There is emerging concordance among experimental, theoretical and observational studies for values of the nuclear symmetry energy parameters and neutron star radii. This will reduce uncertainties from astrophysical simulations of supernovae, neutron star mergers, proto-neutron stars and cooling neutron stars.

This work was initated by the U.S. DOE-funded Topical Collaboration at Los Alamos and partially supported by the U.S. DOE grant DE-AC02-87ER40317.

---

[*] E-mail: lattimer@mail.astro.sunysb.edu

[†] E-mail: ylim@mail.astro.sunysb.edu

[1] A. W. Steiner, M. Prakash, J. M. Lattimer and P. Ellis, Phys. Rep. **411**, 325 (2005); J. M. Lattimer and M. Prakash, Phys. Rept. **442**, 109 (2007).

[2] F. D. Swesty, J. M. Lattimer and E. S. Myra, Astrophys. J. **425**, 195 (1994).

[3] L. F. Roberts et al., Phys. Rev. Lett. **108**, 061103 (2012).

[4] J. M. Lattimer and M. Prakash, Astrophys. J. **550**, 426 (2001).

[5] J. M. Lattimer and B. F. Schutz, Astrophys. J. **629**, 979 (2005).

[6] A. Bauswein and H.-T. Janka, Phys. Rev. Lett. **108**, 011101 (2012); B. D. Lackey, K. Kyutoku, M. Shibata, P. R. Brady and J. L. Friedman, arXiv1109:3402 (2011).

[7] J. M. Lattimer, C. J. Pethick, M. Prakash and P. Haensel, Phys. Rev. Lett. **66**, 2701 (1991).

[8] B. Link, R. I. Epstein and J. M. Lattimer, Phys. Rev. Lett. **83**, 3362 (1999).

[9] J. M. Lattimer, K. A. van Riper, M. Prakash and M. Prakash, Astrophys. J. **425**, 802 (1994).

[10] D. Page and S. Reddy, Thermal and Transport Properties of the Neutron Star Inner Crust, in *Neutron Star Crust*, ed. C. A. Bertulani and J. Piekarewicz, arXiv:1201.5602.

[11] K. Hurley et al., Nature **434**, 1098 (2005); C. Thompson and R. C. Duncan, Astrophys. J. **561**, 980 (2001); L. Samuelsson and N. Andersson, MNRAS **374**, 256 (2007).

[12] T. Li et al., Phys. Rev. C **81**, 034309 (2010).

[13] L.-W. Chen, C. M. Ko and B.-A. Li, Phys. Rev. C **76**, 054316 (2007).

[14] M. Centelles et al., Phys. Rev. Lett. **102**, 122502 (2009).

[15] J. M. Lattimer, in *The Structure and Evolution of Neutron Stars*, ed. D. Pines, R. Tamagaki and S. Tsuruta (Addison-Wesley, New York), p. 50 (1992); J. M. Lattimer, in *Nuclear Equation of State*, ed. A. Ansari and L. Satpathy (World Scientific, Singapore), p. 83 (1996).

[16] W. M. Myers and W. J. Swiatecki, Nucl. Phys. A **81**, 1 (1966).

[17] Y. Lim and J. M. Lattimer, in preparation (2012).

[18] J. M. Lattimer and F. D. Swesty, Nucl. Phys. A **535**, 331 (1991).

[19] W. M. Myers and W. J. Swiaecki, Ann. Phys. **55**, 395 (1969).

[20] M. Kortelainen et al., Phys. Rev. C **82**, 024313 (2010).

[21] L.-W. Chen et al., Phys. Rev. C **82**, 024321 (2010).

[22] S. Abrhamyan et al., arXiv:1201.2568 (2012).

[23] E. Lipparini and S. Stringari, Phys. Rep. **175**, 103 (1989).

[24] A. Tamii et al., Phys. Rev. Lett. **107**, 062502 (2011).

[25] J. Piekarewicz et al., arXiv:1201.3807 (2012).

[26] L. Trippa, G. Coló and E. Vigezzi, Phys. Rev. C **77**, 061304 (2008).

[27] M. B. Tsang et al., Phys. Rev. Lett. **102**, 122701 (2009).

[28] A. Carbone et al., Phys. Rev. C **81** ,041301 (2010).

[29] I. Daoutidis and S. Goriely, Phys. Rev. C **84**, 027301 (2011).

[30] P.-G. Reinhard and W. Nazarewicz, Phys. Rev. C **81**, 051303 (2010).

[31] P. Danielewicz and J. Lee, Int. J. Mod. Phys. E **18**, 892 (2009).

[32] D. V. Shetty, S. J. Yennello and G. A. Souliotis, Phys. Rev. C **76**, 024606 (2007).

[33] K. Hebeler, J. M. Lattimer, C. J. Pethick and A. Schwenk, Phys. Rev. Lett. **105**, 161102 (2010)

[34] S. Gandolfi, J. Carlson and S. Reddy, Phys. Rev. C, in press; arXiv:1101.1921 (2012).

[35] C. O. Heinke, G. B. Rybicki, R. Narayan and J. E. Grindlay, Astrophys. J. **644**, 1090 (2006); N. A. Webb and D. Barret, Astrophys. J. **671**, 727 (2007); S. Guillot, R. E. Rutledge and E. F. Brown, Astrophys. J. **732**, 88 (2011).

[36] T.E. Strohmayer and L. Bildsten, in *Compact Stellar X-ray Sources*, ed. W. Lewin and M. van der Klis (Cambridge University Press, Cambridge, 2004), p. 113.

[37] A. W. Steiner, J. M. Lattimer and E. F. Brown, Astrophys. J. **722**, 33 (2010).

[38] D. A. Leahy, S. M. Morsink and Y. Chou, Astrophys. J. **742**, 17 (2011).